Scientific Research Publishing

Open Journal of Applied Sciences, 2022, 12, 2081-2095
https://www.scirp.org/journal/ojapps
ISSN Online: 2165-3925
ISSN Print: 2165-3917

The Scattering of SH Wave in a Nano Hole Embedded the Infinite Inhomogeneous Medium

Yongqiang Sun[1], Tong Shang[2]

[1]Department of Basic Education Research, Xinjiang University of Science and Technology, Kuerle, China
[2]Advanced Structural Technology Research Institute, Beijing Institute of Technology, Beijing, China
Email: 15009313419@163.com, st13939050446@163.com

How to cite this paper: Sun, Y.Q. and Shang T. (2022) The Scattering of SH Wave in a Nano Hole Embedded the Infinite Inhomogeneous Medium. *Open Journal of Applied Sciences*, **12**, 2081-2095.
https://doi.org/10.4236/ojapps.2022.1212144

Received: October 31, 2022
Accepted: December 25, 2022
Published: December 28, 2022

Abstract

Scattering of the shear waves by a nano-sized cylindrical hole embedded the inhomogeneous is investigated in this study. The Helmholtz equation with a variable coefficient is transformed the standard Helmholtz equation by the complex function method and the conformal mapping method. By wave function expanding method, the analytical expressions of the displacement field and stress field in the inhomogeneous medium are obtained. Considering the surface effect and using the generalized Young-Laplace equation, we obtain the boundary conditions at nano arbitrary-shaped hole, then the field equations satisfying boundary conditions are attributed to solving a set of infinite algebraic equations. Numerical results show that when the radius of the cylindrical cavity shrinks to nanometers, surface energy becomes a dominant factor that affects the dynamic stress concentration factor (DSCF) around the cylindrical cavity. The influence the density variation of the inhomogeneity on the DSCF is discussed at the same time.

Keywords

Conformal Mapping Method, Power-Law Variation Inhomogeneous Medium, Helmholtz Equation with Variable Coefficient, Dynamic Stress Concentration Factor, Nano-Sized Cylindrical Cavity

1. Introduction

The study of wave propagation in complex media is a recognized challenge that has attracted the attention of many researchers in recent years. Since the continuous medium has many defects, including cavities, inclusion, and crack, so the scattering of elastic waves and the dynamic stress concentration around the defects are often discussed in wave research. Pao and Mow [1] studied the dynamic

stress concentration problem for all types of defects. Similar issues were also discussed based on complex function theory by Liu *et al.* [2].

Since most media are not homogeneous, the propagation of waves in inhomogeneous media has attracted widespread attention. The basic solution of SH wave propagation in inhomogeneous and anisotropic media can be directly derived by analytical methods [3]. Taking into account the inhomogeneity and anisotropy of the medium, the expressions of the incident wave and the scattered wave are given in the calculations. As a simplified condition, it is also a feasible method to divide the continuous inhomogeneous medium into multiple layers. Let the multi-layered medium consist of periodically repeated fundamental wave plates with a small thickness to achieve the wave speed in the inhomogeneous medium [4]. The study of elastic waves scattered by inhomogeneous circular tubes is of great significance in materials science [5]. Assuming the tube is linearly inhomogeneous, the finite Fourier transform is used to solve the governing equation. Furthermore, this study provides a feasible method for researching the SH waves scattered by underground inhomogeneous lined tunnels. The auxiliary function method is used to analyze the motion of wave in a uniform and inhomogeneous medium and discussed the wave field, stress distribution, and far-field behavior [6] [7] [8]. Yang and Liu applied the conformal mapping method, the closed solution of SH wave propagation in variable speed inhomogeneous media was also studied. Through the normalized control equation, the dynamic stress concentration around the inclusions was analyzed [9] [10].

The main feature of modern composite materials and nanocomposites is that there is an obvious interphase area between the nano inclusion and the matrix. This area may be created due to the manufacturing process, or it may be deliberately introduced between the two main stages to increase the enhanced performance of the material. This article mainly considers the influence of the surface/interface on the nanoscale. Gurtin and Murdoch first established a continuum mechanical model including free surface stress [11] [12] [13]. The stress model assumes that nanostructures are composed of blocks and free surfaces with different moduli [14]. The model agrees well with the atomic simulation results observed by Miller and Shenoy [15] [16]. There are some reports on the effect of surface energy on elastic wave scattering. Fang's team considered the multiple scattering of electro elastic waves of two piezoelectric nanofibers in the piezoelectric matrix and obtained the dynamic stress at the interface [17]. Cai and Wei studied the effect of the surface/interface of a two-dimensional photonic crystal with periodically arranged nanopores on the dispersion relationship and bandgap performance [18]. The surface elasticity theory was used to consider the surface stress effect, and the nontraditional boundary conditions of the nanopore surface are derived. Based on the theory of surface/interface elasticity, Fang's team studied the effect of surface/interface on the dynamic stress of the nano inhomogeneities of two interacting cylinders under compression waves [19]. The scattering of plane compression waves by a series of nano inclusions containing circular cavities is reported by Wang. This report also used the sepa-

ration variable method to obtain the stress field in the matrix and the cavity interface. The results showed that the surface effect depends on the location, size, and material of the inclusions [20]. Ou's team used the wave function expansion method to solve the scattering of plane elastic waves by coated fibers with surface effects at the nanoscale. The influence of surface effects on the scattering of compressional waves in the problem of semi-cylindrical nano-holes is also studied. The results show that the size of holes, inclusions and the surface/interface effect greatly affect the dynamic stress concentration factor, especially at the nanometer scale, the effect of surface/interface effects is more obvious [21] [22].

This paper studies the scattering of SH waves in inhomogeneous infinite body at the nanometer scale. The inhomogeneity of the medium is reflected by the variable wave number that changes along the radial direction with the power law. First, based on the principle of homogenization, the general conformal transformation method is used to transform the Helmholtz equation with variable coefficients into the standard Helmholtz equation. Then, the complex function method is used to determine the dynamic displacement and stress field in the complex coordinate system. Finally, numerical calculation shows the influence of wave number, surface parameters and media inhomogeneity parameters on the dynamic stress distribution around the cylindrical cavity.

2. Problem Formulation

2.1. Elastic Wave Motion Equation and Stress and Displacement Relations

The classical Navier equation controls the motion of wave in a homogeneous isotropic elastic medium. This equation can be written as [1]

$$\left(\lambda+\mu\right)\nabla\nabla\cdot\boldsymbol{u}+\mu\nabla^2\boldsymbol{u}=\rho\ddot{\boldsymbol{u}} \tag{1}$$

where $\boldsymbol{u}$ is the displacement vector, and ∇ is the gradient operator.

In this paper, we study the inhomogeneous medium whose density changes with spatial coordinates, Equation (1) can be expressed as

$$\left(\lambda+\mu\right)\nabla\nabla\cdot\boldsymbol{u}+\mu\nabla^2\boldsymbol{u}=\rho\left(x\right)\ddot{\boldsymbol{u}} \tag{2}$$

Because of the density changes, we can introduce commonly used displacement components

$$\boldsymbol{u}=\boldsymbol{\varphi}+\boldsymbol{\psi} \tag{3}$$

where φ and ψ represent scalar and vector displacement potentials, respectively.

At the same time φ and ψ satisfy the following relationship

$$\nabla\times\varphi=0,\quad \nabla\cdot\psi=0 \tag{4}$$

Introduce Equation (4) into Equation (2), the governing equation can be expressed as

$$\left(\lambda+\mu\right)\nabla\nabla\cdot\left(\varphi+\psi\right)+\mu\nabla^2\left(\varphi+\psi\right)=\rho\left(x\right)\left(\ddot{\varphi}+\ddot{\psi}\right) \tag{5}$$

The energy density equation is

$$\nabla^2 \boldsymbol{u} = \nabla(\nabla \cdot \boldsymbol{u}) - \nabla \times (\nabla \times \boldsymbol{u}) \tag{6}$$

Simultaneous Equation (5) and Equation (6), we can obtain

$$(\lambda + 2\mu)\nabla^2 \psi + \mu \nabla^2 \varphi = \rho(x)(\ddot{\varphi} + \ddot{\psi}) \tag{7}$$

Under the condition of simple harmonic time, two variable coefficient Helmholtz equations can be obtained

$$\nabla^2 \varphi + k_p^2(x)\varphi = 0 \tag{8}$$

$$\nabla^2 \psi + k_s^2(x)\psi = 0 \tag{9}$$

where $k_p = \omega / c_p$, $k_s = \omega / c_s$ are the wave numbers of compressional wave and shear wave, respectively.

In Cartesian coordinate system, the wave equation of variable coefficient of the isotropic infinite inhomogeneous medium can be written as

$$\nabla^2 \varphi(\boldsymbol{x}) + k^2(\boldsymbol{x})\varphi(\boldsymbol{x}) = 0 \tag{10}$$

where ∇^2 is the Laplacian, $\boldsymbol{x} = (x, y)$ is the position vector, $k(\boldsymbol{x}) = \omega / c(\boldsymbol{x})$ means the wave number of shear wave, ω is the circular frequency of the displacement $\varphi(\boldsymbol{x})$, $c(\boldsymbol{x}) = \sqrt{\mu(\boldsymbol{x}) / \rho(\boldsymbol{x})}$ is the velocity of shear wave, ρ and μ are the density and the shear modulus of the inhomogeneous medium.

The stress component can be expressed as

$$\tau_{xz} = \mu \frac{\partial \varphi}{\partial x}, \quad \tau_{yz} = \mu \frac{\partial \varphi}{\partial y} \tag{11}$$

Introducing complex variable $z = x + iy$ and $\overline{z} = x - iy$ to Equation (10) and Equation (11). These two equations can be written as follows

$$\frac{\partial^2 \varphi}{\partial z \partial \overline{z}} + \frac{1}{4} k^2(z, \overline{z})\varphi = 0 \tag{12}$$

$$\tau_{rz} = \mu \left(\frac{\partial \varphi}{\partial z} \mathrm{e}^{i\theta} + \frac{\partial \varphi}{\partial \overline{z}} \mathrm{e}^{-i\theta} \right) \tag{13}$$

$$\tau_{\theta z} = i\mu \left(\frac{\partial \varphi}{\partial z} \mathrm{e}^{i\theta} - \frac{\partial \varphi}{\partial \overline{z}} \mathrm{e}^{-i\theta} \right) \tag{14}$$

2.2. Description of the Inhomogeneity

The model of an infinite inhomogeneous medium with a cylindrical cavity is shown in **Figure 1**. Assuming the elastic medium is inhomogeneous and isotropic, the origin of the polar coordinate system is located in the center of the cylindrical cavity. The time harmonic wave propagates as the incident waves along the positive direction of the *x*-axis in a radially inhomogeneous medium. It is assumed that the mass density varies continuously in the radial direction and approaches uniform value at distance far from the origin.

According to the power-law function, the fluctuation of the media density is expressed as

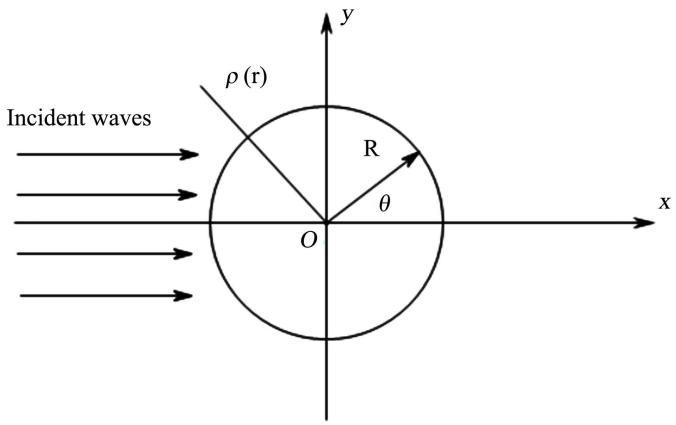

Figure 1. The model of SH-wave horizontal incidence in a radial inhomogeneous infinite body.

$$\rho(r) = \rho_0 \beta^2 r^{2(\beta-1)} \tag{15}$$

where β is the inhomogeneous parameter of the inhomogeneous medium, and ρ_0 is the reference density.

2.3. Transformation of the Governing Equation

Equation (11) written in the cylindrical coordinate system takes the form as

$$r^2 \frac{\partial^2 \varphi}{\partial r^2} + r \frac{\partial \varphi}{\partial r} + \frac{\partial^2 \varphi}{\partial \theta^2} + r^2 k^2 (r,\theta) \varphi = 0 \tag{16}$$

Based on the relationship between k and ρ, Equation (15) can be written as

$$k(r) = k_0 \cdot \beta r^{\beta-1} \tag{17}$$

$k_0 = \omega / c_0$ is the reference wave number, and c_0 is the velocity of reference shear wave. Equation (16) can be expressed as

$$\frac{\partial^2 \varphi}{\partial r^2} + \frac{1}{r} \frac{\partial \varphi}{\partial r} + \frac{1}{r^2} \frac{\partial^2 \varphi}{\partial \theta^2} + \beta^2 r^{2(\beta-1)} k_0^2 \varphi = 0 \tag{18}$$

In the complex coordinate system $(z, \overline{z})$, Equation (18) can be rewritten as

$$\frac{\partial^2 \varphi}{\partial z \partial \overline{z}} + \frac{1}{4} \beta^2 (z\overline{z})^{\beta-1} k_0^2 \varphi_0 = 0 \tag{19}$$

To normalize the Helmholtz equation with variable coefficients, a new transformation variable is introduced

$$\zeta = z^{\beta}, \quad \overline{\zeta} = \overline{z}^{\beta} \tag{20}$$

Substituting Equation (20) into Equation (19), the wave equation is normalized into a Helmholtz equation with a constant coefficient

$$\frac{\partial^2 \varphi}{\partial \zeta \partial \overline{\zeta}} + \frac{1}{4} k_0^2 \varphi = 0 \tag{21}$$

Substituting Equation (20) into Equation (13) and Equation (14), the corresponding stress can be expressed as

$$\tau_{rz} = \mu\beta\left(\frac{\partial\varphi}{\partial\zeta}z^{\beta-1}e^{i\theta} + \frac{\partial\varphi}{\partial\bar{\zeta}}\bar{z}^{\beta-1}e^{-i\theta}\right) \tag{22}$$

$$\tau_{\theta z} = i\mu\beta\left(\frac{\partial\varphi}{\partial\zeta}z^{\beta-1}e^{i\theta} - \frac{\partial\varphi}{\partial\bar{\zeta}}\bar{z}^{\beta-1}e^{-i\theta}\right) \tag{23}$$

3. Fields of Displacement and Stress

In the complex ζ-plane, the incident wave horizontal propagation can be written as

$$\varphi^{Inc.} = \varphi_0 \exp\left[ik_0\left(\zeta + \bar{\zeta}\right)/2\right] \tag{24}$$

where φ_0 is the amplitude of the incident wave. The $e^{-i\omega t}$ is time-dependent term [23].

Introducing Equation (24) into Equation (22) and Equation (23), the stress components of the incident wave are

$$\tau_{rz}^{(i)} = \frac{i\mu\beta k_0\varphi_0}{2}\left(z^{\beta-1}e^{i\theta} + \bar{z}^{\beta}e^{-i\theta}\right)\exp\left[\frac{ik_0}{2}\left(\zeta + \bar{\zeta}\right)\right] \tag{25}$$

$$\tau_{\theta z}^{(i)} = -\frac{\mu\beta k_0\varphi_0}{2}\left(z^{\beta-1}e^{i\theta} - \bar{z}^{\beta-1}e^{-i\theta}\right)\exp\left[\frac{ik_0}{2}\left(\zeta + \bar{\zeta}\right)\right] \tag{26}$$

The scattering field caused by a cylindrical in an inhomogeneous infinite medium satisfying Equation (21) can be expressed as

$$\varphi^{sca} = \sum_{n=-\infty}^{\infty} A_n H_n^{(1)}\left(k_0|\zeta|\right)\left(\frac{\zeta}{|\zeta|}\right)^n \tag{27}$$

where A_n is unknown coefficient, $H_n^{(1)}(\cdot)$ is the nth-order Hankel function of the first kind.

Substituting Equation (27) into Equation (22) and Equation (23), the stress components of the scattering wave are

$$\begin{aligned}\tau_{rz}^{(s)} = \frac{\beta\mu k_0}{2}\sum_{n=-\infty}^{\infty} A_n \Bigg\{ & H_{n-1}^{(1)}\left(k_0|\zeta|\right)\left(\frac{\zeta}{|\zeta|}\right)^{n-1}\cdot z^{\beta-1}e^{i\theta} \\ & - H_{n+1}^{(1)}\left(k_0|\zeta|\right)\left(\frac{\zeta}{|\zeta|}\right)^{n+1}\cdot \bar{z}^{\beta-1}e^{-i\theta}\Bigg\}\end{aligned} \tag{28}$$

$$\begin{aligned}\tau_{\theta z}^{(s)} = \frac{i\beta\mu k_0}{2}\sum_{n=-\infty}^{\infty} A_n \Bigg\{ & H_{n-1}^{(1)}\left(k_0|\zeta|\right)\left(\frac{\zeta}{|\zeta|}\right)^{n-1}\cdot z^{\beta-1}e^{i\theta} \\ & + H_{n+1}^{(1)}\left(k_0|\zeta|\right)\left(\frac{\zeta}{|\zeta|}\right)^{n+1}\cdot \bar{z}^{\beta-1}e^{-i\theta}\Bigg\}\end{aligned} \tag{29}$$

4. Surface Elasticity and the Resulting Boundary Conditions

To incorporate the surface/interface effect into this study, the Gurtin-Murdoch surface elastic model was used in this paper. This model considers the interface

as a film of negligible thickness, it adheres to the surrounding bulk material without sliding. The equilibrium and constitutive equations in the bulk of the solid can be written as

$$\tau_{ij,j} = \rho \frac{\partial^2 u_i}{\partial t^2} \tag{30}$$

$$\tau_{ij} = 2\mu\left(\varepsilon_{ij} + \frac{\nu}{1-2\nu}\varepsilon_{kk}\delta_{ij}\right) \tag{31}$$

In which t is the time, ρ is the mass density of the material, μ and ν are shear modulus and Poisson's ration, respectively. τ_{ij} and ε_{ij} are the stress tensor and strain tensor in the bulk material.

The relationship between the strain tensor and the displacement vector u_i is

$$\varepsilon_{ij} = \frac{1}{2}\left(\frac{\partial u_i}{\partial x_j} + \frac{\partial u_j}{\partial x_i}\right) \tag{32}$$

The equilibrium equations on the surface can be expressed as (22)

$$t_\alpha + \tau^s_{\beta\alpha,\beta} = 0, \quad \tau_{ij} n_i n_j = \tau^s_{\alpha\beta}\kappa_{\alpha\beta} \tag{33}$$

n_i is the normal vector of the surface, t_α denotes the negative of the tangential component of the traction. $t_i = \tau_{ij} n_j$ in the x_α direction, $\kappa_{\alpha\beta}$ is the curvature of the surface.

The surface stresses of the anisotropic surface are given as [24] [25].

$$\tau^s_{\alpha\beta} = 2\mu^s \varepsilon_{\alpha\beta} + \lambda^s \varepsilon_{\gamma\gamma}\delta_{\alpha\beta} \tag{34}$$

$\delta_{\alpha\beta}$ is the Kronecker delta, $\varepsilon_{\alpha\beta}$ is the second-rank tensor of surface strain, λ^s and μ^s are surface elastic constants.

For a circular hole with radius $r = a$, according to Equation (33) and Equation (34), we find

$$\tau_{rz} = -\frac{1}{a}\frac{\partial \tau^s_{\theta z}}{\partial \theta}, \quad \tau^s_{\theta z} = 2\mu^s \varepsilon_{\theta z} \tag{35}$$

The stress boundary conditions around the circular hole can be obtained from Equation (35)

$$\tau_{rz} = -s\frac{\partial \tau_{\theta z}}{\partial \theta} \tag{36}$$

where

$$s = \frac{\mu^s}{\mu a} \tag{37}$$

s is a dimensionless parameter that reflects the effect of the surface/interface on the nanoscale. It is seen from Equation (25) that the radius of the hole is reduced to nanoscale, s is visible and surface effects should be taken into account in the analysis. However, for a macroscopic hole with a big radius, $s \to 0$, the surface/interface effect can be neglected [25].

The boundary condition of the space boundary and the unit circle hole are as follows

$$\tau_{rz}(r,\theta) = -s\frac{\partial \tau_{\theta z}}{\partial \theta} \tag{38}$$

$$\tau_{rz}(r,\theta) = \tau_{rz}^{(i)} + \tau_{rz}^{(s)} = 0 \tag{39}$$

Substituting Equations (25)-(29) into Equation (38) and Equation (39), we find

$$\sum_{n=-\infty}^{\infty} A_n \varepsilon_n + \varepsilon = 0 \tag{40}$$

Multiplying both side of Equation (28) by $e^{-im\theta}$ and integrating between the interval $(-\pi,\pi)$, there is

$$\sum_{n=-\infty}^{\infty} A_n \varepsilon_n^m + \varepsilon^m = 0,\ \ m = n = 0,\pm 1,\pm 2,\cdots \tag{41}$$

In which

$$\varepsilon_n^m = \frac{1}{2\pi}\int_{-\pi}^{\pi} \varepsilon_n e^{-im\theta} d\theta,\ \ \varepsilon^m = \frac{1}{2\pi}\int_{-\pi}^{\pi} \varepsilon e^{-im\theta} d\theta \tag{42}$$

A set of infinite algebraic equation for unknown constants A_n will be obtained from Equation (42).

5. Numerical Results and Discussion

The dynamic stress concentration factor (DSCF) due to seismic waves is an important parameter for engineering applications. The SH-wave induced DSCF is calculated as

$$\text{DSCF} = \left|\frac{\tau_{\theta z}}{\tau_0}\right| \tag{43}$$

where $\tau_0 = \mu\beta k_0 \varphi_0$ is the maximum amplitude of the incident stress.

To verify the correctness of this paper, $s = 0$, the current nanosized cylindrical cavity is reduced to the classical cavity problem without surface effects in **Figure 2**. These results are exactly the same as references [8].

It can be seen from **Figure 3**, the interaction between the symmetry of the model and the horizontal incidence of SH waves makes the DSCF is x axial symmetry. When $0 < s < 2$, the value of DSCF decreases gradually with the increase of surface parameter *s*, the changing trend of $s = 0$ and $s = 0.1$ are not obvious. Compared with the macroscopic case, the dynamic stress concentration factor at nanometer scale is smaller.

From **Figure 4**, the DSCF values decrease gradually when $0 < s < 2$, and they change consistently when $s = 0.5$ and $s = 2$. Compared with **Figure 3**, the high frequency incident wave peaks appear at $\theta = \pi$ and the wave troughs appear at $\theta = 0$.

As can be seen from **Figure 5**, the DSCF values decrease gradually when $0 < s < 2$, and the value of DSCF decreases sharply when $s = 2$. Compared with **Figure 3**, the values near $\theta = 0$ and $\theta = \pi$ decrease first then increase with the increase of inhomogeneious parameter β.

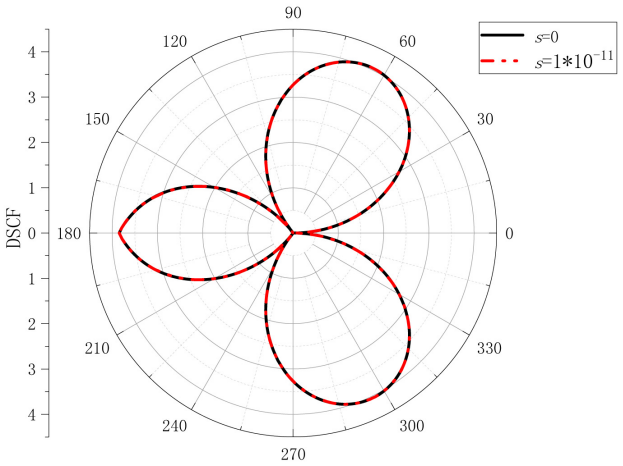

Figure 2. Verification of DSCF by the degeneration procedure with $\beta R = 1.4$.

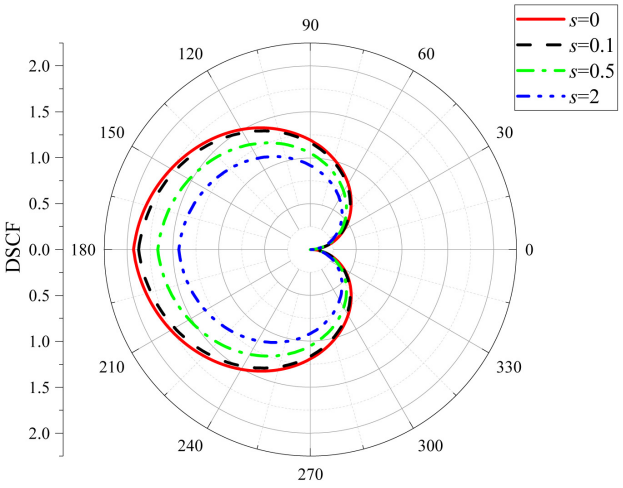

Figure 3. Effect of surface parameter s on DSCF near a circle cavity for $\beta R = 0.4$, $k_0 R = 0.1$.

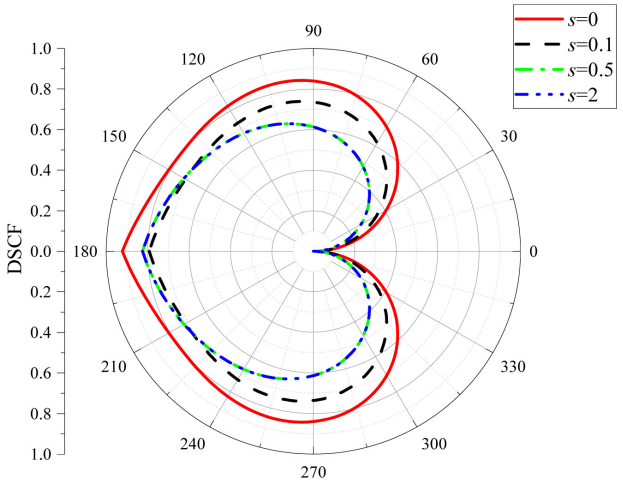

Figure 4. Effect of surface parameter s on DSCF near a circle cavity for $\beta R = 0.4$, $k_0 R = 2$.

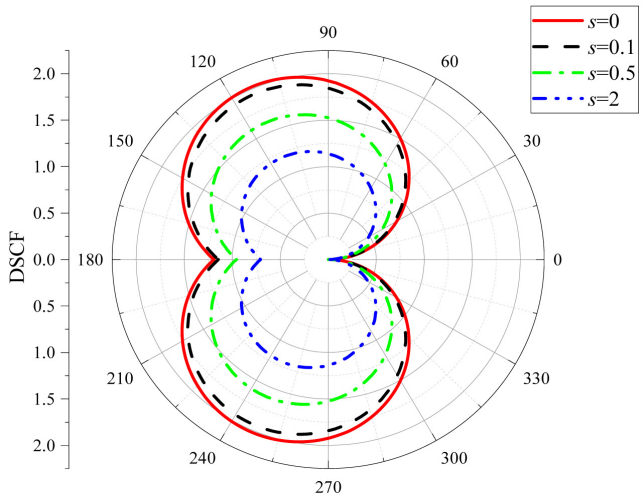

Figure 5. Effect of surface parameter s on DSCF near a circle cavity for $\beta R = 0.8$, $k_0 R = 0.1$.

It can be seen from **Figure 6** that the DSCF changes complicatedly with the increase of surface parameter s, and there is no certain rule. When $s = 2$, the DSCF value varies greatly, with multiple peaks, and the maximum value of DSCF occurs at angles $\theta = \pi/6$ and $\theta = 5\pi/6$. When the wavenumber is constant and the nonuniform parameter β doubles as compared to **Figure 4**, the DSCF value also doubles or so.

It can be seen from **Figure 7** that the DSCF decreases with the increase of surface parameter s. Compared with $s = 2$ and $s = 0$, the maximum value of DSCF decreases by more than half. In the vicinity of $\theta = 0$ and $\theta = \pi$, the value of DSCF decreases first then increases. Compared with **Figure 5**, with the increase of β, the maximum value of DSCF moves from the front to the back of the wave.

As **Figure 8** shows, DSCF increase with the growth of surface parameter s. In the case of $s = 0$ and $s = 0.1$, the DSCF has no change, but in the case of $0.5 < s < 2$, the DSCF is increase. There are many peaks and troughs. Relative to **Figure 7**, the DSCF changes occur primarily at the high incident wave surface.

It can be seen from **Figure 9** that the DSCF decreases with the increase of surface parameter s. Compared to $s = 0$, $s = 2$ reduces the DSCF value by half, with the largest values occurring at $\theta = \pi/3$ and $\theta = 5\pi/6$. Relative to **Figure 3**, the distribution of DSCF shifts from the front to the back when β is increased by three times, and the maximum value increases.

Figure 10 shows that as the surface parameter s increases, the dynamic stress concentration factor increases, and the wave-facing surface appears with multiple peaks and valleys. The wave phenomena of DSCF shifts from wave back to wave head-on with the increase of s. When the surface parameters and incident wave number are constant, compared with **Figure 8**, the maximum value of the dynamic stress concentration factor increases with the increase of β, and it is mainly distributed on the back of the wave.

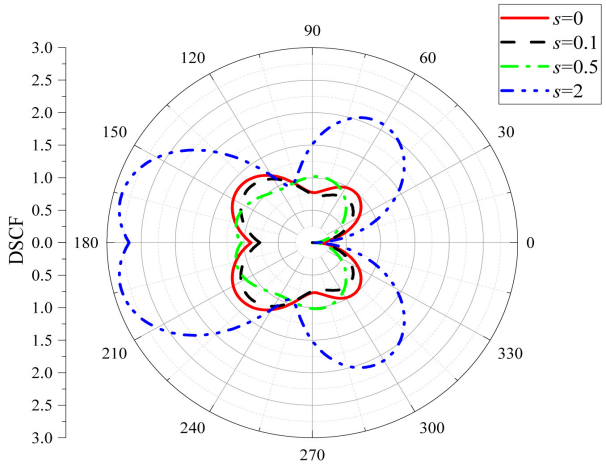

Figure 6. Effect of surface parameter s on DSCF near a circle cavity for $\beta R = 0.8$, $k_0 R = 2$.

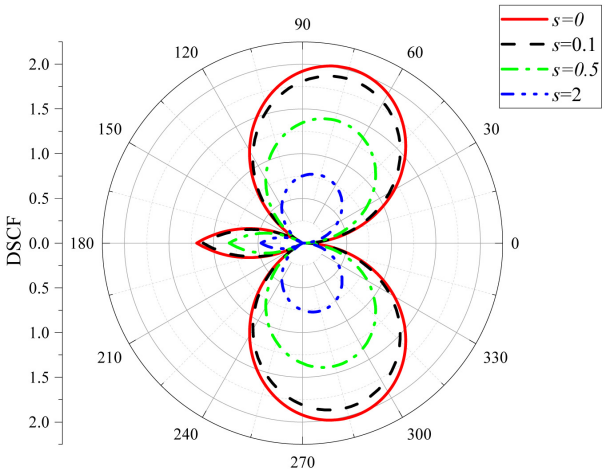

Figure 7. Effect of surface parameter s on DSCF near a circle cavity for $\beta R = 1.2$, $k_0 R = 0.1$.

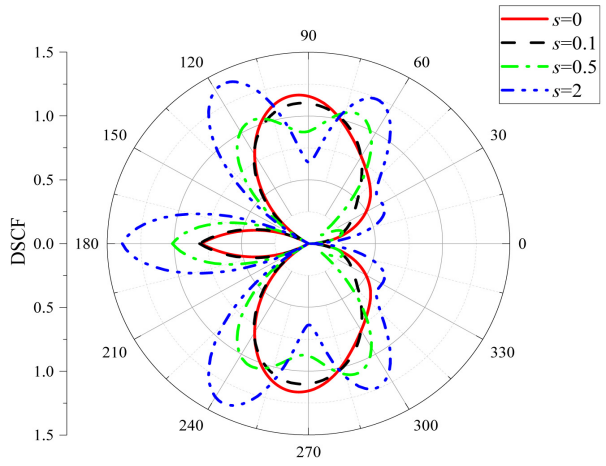

Figure 8. Effect of surface parameter s on DSCF near a circle cavity for $\beta R = 1.2$, $k_0 R = 2$.

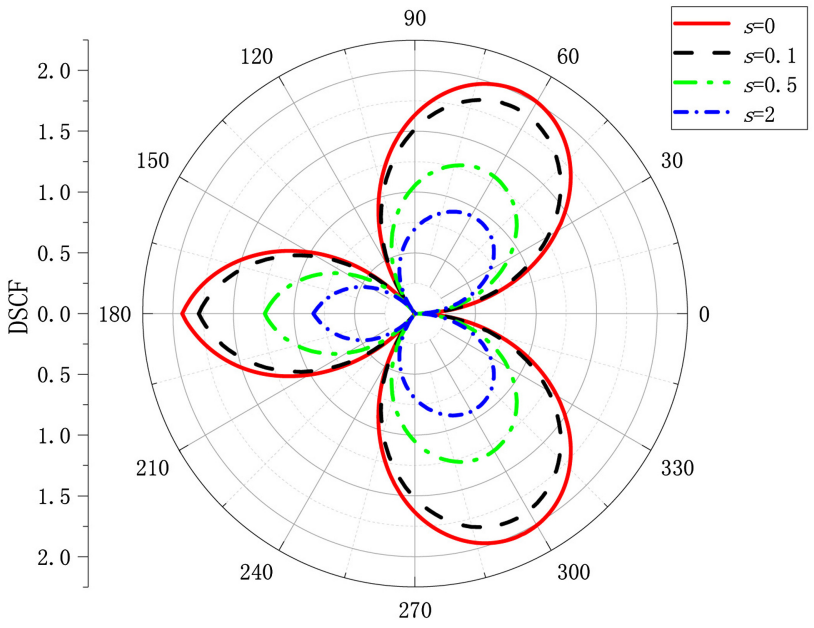

Figure 9. Effect of surface parameter s on DSCF near a circle cavity for $\beta R = 1.4$, $k_0 R = 0.1$.

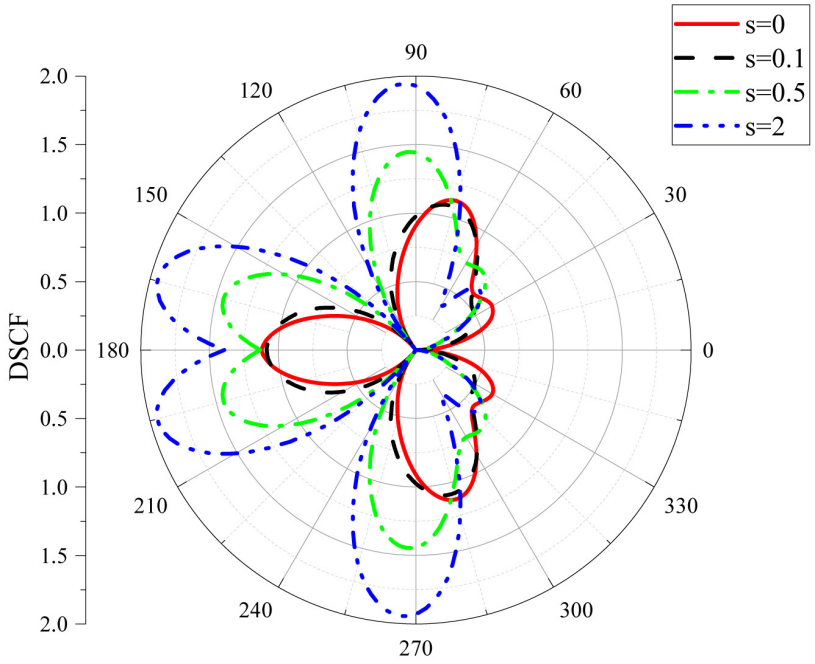

Figure 10. Effect of surface parameter s on DSCF near a circle cavity for $\beta R = 1.4$, $k_0 R = 2$.

It can be seen from **Figure 11** that at point $0 < \beta < 0.5$, the distribution of DSCF mainly appears on the front of the wave, and the maximum value is obtained at point $\theta = \pi$, with $0.6 < \beta < 1.4$. The dynamic stress concentration factor near the x-axis first decreases then increases, while at the back of the wave, the fluctuation range is becoming obvious.

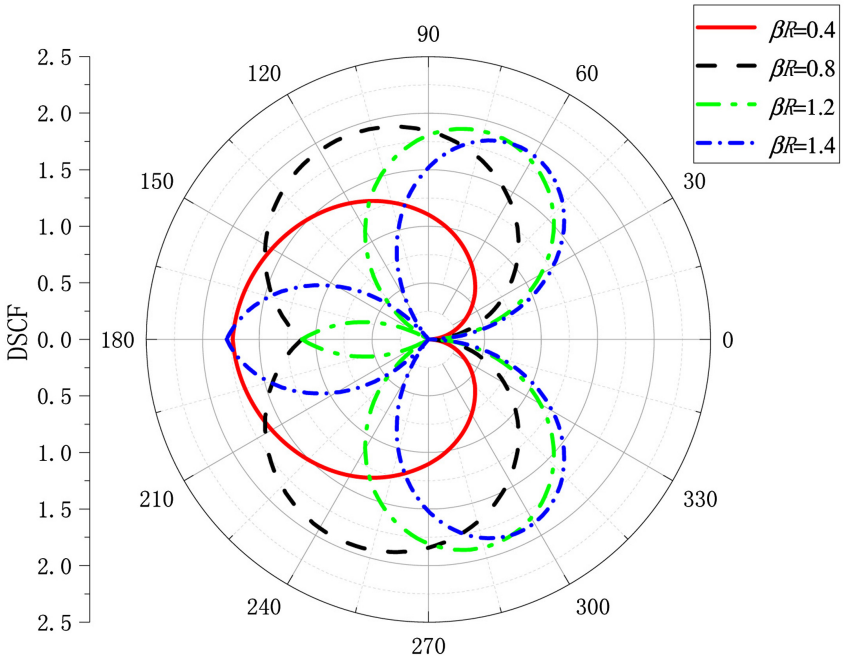

Figure 11. Effect of surface parameter $s = 0.1$ on DSCF near a circle cavity for $k_0 R = 0.1$.

6. Conclusions

The scattering of SH waves from a cylindrical cavity on a nanometer scale in a radially inhomogeneous isotropic medium is studied in this paper based on the complex function method and the theory of surface/interface elasticity. For an inhomogeneous medium, it is assumed that the mass density changes continuously in the radial direction. It is close to a uniform value at a distance away from the origin. To solve the variable coefficient governing equation, the conformal mapping method is used. Applying the boundary conditions at the cavity, the wave fields and the corresponding stresses are solved. Finally, the DSCF around the cylindrical cavity is obtained and analyzed, and some conclusions are summarized:

1) The distribution of DSCF is mainly influenced by inhomogeneous parameter, surface parameter, and reference wave number. The increase of β, s and $k_0 R$ causes the distribution of DSCF to be complicated and may change the position of the maximum of DSCF;

2) When $k_0 R$ is 0.1, DSCF is mainly distributed on the face of wave, and the maximum appears at $\theta = \pi$. With the increase of $k_0 R$ near the x-axis first decreases and then increases;

3) When $k_0 R$ is 2, the maximum value of DSCF appears on the back wave surface. In high-frequency situations, the distribution of DSCF fluctuates.

Acknowledgements

This work is supported by the Science and Technology Research Center of Xinjiang University of Science and Technology (Grant NO. 2022KYPT17).

Conflicts of Interest

The author declares no conflicts of interest regarding the publication of this paper.

References

[1] Pao, Y.H., Mow, C.C. and Achenbach, J.D. (1973) Diffraction of Elastic Waves and Dynamic Stress Concentrations. *Journal of Applied Mechanics*, **40**, 213-219. https://doi.org/10.1115/1.3423178

[2] Liu, D., Gai, B. and Tao, G. (1982) Applications of the Method of Complex Functions to Dynamic Stress Concentrations. *Wave Motion*, **4**, 293-304. https://doi.org/10.1016/0165-2125(82)90025-7

[3] Kowalczyk, S., Matysiak, S.J. and Perkowski, D.M. (2015) On Some Problems of SH Wave Propagation in Inhomogeneous Elastic Bodies. *Journal of Theoretical & Applied Mechanics*, **54**, 1125-1135. https://doi.org/10.15632/jtam-pl.54.4.1125

[4] Kara, H.F. and Aydogdu, M. (2018) Dynamic Response of a Functionally Graded Tube Embedded in an Elastic Medium Due to SH-Waves. *Composite Structures*, **206**, 22-32. https://doi.org/10.1016/j.compstruct.2018.08.032

[5] Ghafarollahi, A. and Shodja, H.M. (2018) Scattering of SH-Waves by an Elliptic Cavity/Crack beneath the Interface between Functionally Graded and Homogeneous Half-Spaces via Multipole Expansion Method. *Journal of Sound and Vibration*, **435**, 372-389. https://doi.org/10.1016/j.jsv.2018.08.022

[6] Liu, Q., Zhao, M. and Chao, Z. (2014) Antiplane Scattering of SH Waves by a Circular Cavity in an Exponentially Graded Half Space. *International Journal of Engineering Science*, **78**, 61-72. https://doi.org/10.1016/j.ijengsci.2014.02.006

[7] Martin, P.A. (2009) Scattering by a Cavity in an Exponentially Graded Half-Space. *Journal of Applied Mechanics*, **76**, 540-545. https://doi.org/10.1115/1.3086585

[8] Hei, B., Yang, Z., Sun, B. and Yao, W. (2015) Modelling and Analysis of the Dynamic Behavior of Inhomogeneous Continuum Containing a Circular Inclusion. *Applied Mathematical Modelling*, **39**, 7364-7374. https://doi.org/10.1016/j.apm.2015.03.015

[9] Liu, *et al.* (2016) Dynamic Analysis of Elastic Waves by an Arbitrary Cavity in an Inhomogeneous Medium with Density Variation. *Mathematics and Mechanics of Solids*: *MMS*, **21**, 931-940. https://doi.org/10.1177/1081286514545906

[10] Gurtin, M.E. and Murdoch, A.I. (1975) A Continuum Theory of Elastic Material Surfaces. *Archive for Rational Mechanics & Analysis*, **57**, 291-323. https://doi.org/10.1007/BF00261375

[11] Morton, *et al.* (1978) Surface Stress in Solids. *International Journal of Solids and Structures*, **14**, 431-440. https://doi.org/10.1016/0020-7683(78)90008-2

[12] Murdoch, A.I. (1976) A Thermodynamical Theory of Elastic Material Interfaces. *Quarterly Journal of Mechanics & Applied Mathematics*, **29**, 245-275. https://doi.org/10.1093/qjmam/29.3.245

[13] Xian, F., *et al.* (2014) Dependence of Youngs Modulus of Nanowires on Surface Effect. *International Journal of Mechanical Sciences*, **81**, 120-125. https://doi.org/10.1016/j.ijmecsci.2014.02.018

[14] Miller, R.E. and Shenoy, V.B. (2000) Size-Dependent Elastic Properties of Nanosized Structural Elements. *Nanotechnology*, **11**, 139. https://doi.org/10.1088/0957-4484/11/3/301

[15] Shenoy, V.B. (2002) Size-Dependent Rigidities of Nanosized Torsional Elements. *International Journal of Solids & Structures*, **39**, 4039-4052. https://doi.org/10.1016/S0020-7683(02)00261-5

[16] Hasheminejad, S.M. and Avazmohammadi, R. (2009) Size-Dependent Effective Dynamic Properties of Unidirectional Nanocomposites with Interface Energy Effects. *Composites Science & Technology*, **69**, 2538-2546. https://doi.org/10.1016/j.compscitech.2009.07.007

[17] Fang, X.Q., Liu, J.X., Dou, L.H. and Chen, M.Z. (2012) Dynamic Strength around Two Interacting Piezoelectric Nano-Fibers with Surfaces/Interfaces in Solid under Electro-Elastic Waves. *Thin Solid Films*, **520**, 3587-3592. https://doi.org/10.1016/j.tsf.2012.01.012

[18] Wei, F., *et al.* (2013) Propagation of Elastic Wave in Nanoporous Material with Distributed Cylindrical Nanoholes. *Science China Physics Mechanics & Astronomy*, **56**, 1542-1550.

[19] Wang, G.F. (2009) Multiple Diffraction of Plane Compressional Waves by Two Circular Cylindrical Holes with Surface Effects. *Journal of Applied Physics*, **105**, 4067. https://doi.org/10.1063/1.3054517

[20] Wang, H., Dong, K., Men, F., Yan, Y.J. and Wang, X. (2010) Influences of Longitudinal Magnetic Field on Wave Propagation in Carbon Nanotubes Embedded in Elastic Matrix. *Applied Mathematical Modelling*, **34**, 878-889. https://doi.org/10.1016/j.apm.2009.07.005

[21] Ou, Z.Y. and Lee, D.W. (2012) Effects of Interface Energy on Scattering of Plane Elastic Wave by a Nano-Sized Coated Fiber. *Journal of Sound & Vibration*, **331**, 5623-5643. https://doi.org/10.1016/j.jsv.2012.07.023

[22] Ou, Z.Y., Liu, C. and Liu, X.W. (2013) Effects of Surface Elasticity on Scattering of P Waves by an Elastic Half-Plane with a Nanosized Semi-Cylindrical Inclusion. *Applied Mechanics & Materials*, **303**-**306**, 2661-2666. https://doi.org/10.4028/www.scientific.net/AMM.303-306.2661

[23] Sharma, P., Ganti, S. and Bhate, N. (2003) Effect of Surfaces on the Size-Dependent Elastic State of Nano-Inhomogeneities. *Applied Physics Letters*, **82**, 535-537. https://doi.org/10.1063/1.1539929

[24] Qi, H., Chen, H., Zhang, X., Zhao, Y. and Xiang, M. (2018) Scattering of SH-Wave by an Elliptical Inclusion with Partial Debonding Curve in Half-Space. *Waves in Random and Complex Media*, **29**, 281-298. https://doi.org/10.1080/17455030.2018.1430407

[25] Sharma, P. and Ganti, S. (2004) Size-Dependent Eshelby's Tensor for Embedded Nano-Inclusions Incorporating Surface/Interface Energies. *Journal of Applied Mechanics*, **72**, 663-671. https://doi.org/10.1115/1.1781177